BEAM-BASED MEASUREMENTS OF THE CBETA MAIN LINAC CAVITY ALIGNMENT

C. Gulliford, N. Banerjee, A. Bartnik, J. Crittenden, P. Quigley,
Cornell University, Ithaca, NY, USA
J. S. Berg,
BNL, Upton, New York, USA,

Abstract

This work presents the results of beam based measurements of the individual cavity offsets and tilts taken during the CBETA Fractional Arc Test. This was achieved using a pair of corrector magnets to scan the beam position on the BPM just upstream of the linac while keeping the beam's angle constant. With one cavity turned on at a time (all others off), the cavity phased was scanned 360 deg and the resulting position changed recorded on a downstream BPM just after the linac. Fourier analysis of the linear dynamics through the cavity, as well as the transfer matrix elements available from particle tracking, was then used to compute the cavity offset and tilt. This procedure was performed for each of the six main linac cavities, and resulting in a weighted average cavity offset of roughly 4.0 mm.

INTRODUCTION

The Cornell-BNL Energy recovery linac Test Accelerator (CBETA) [1], a 4-pass, 150 MeV ERL utilizing a Nonscaling Fixed Field Alternating-gradient (NS-FFA) permanent magnet return loop [2], is currently under design and construction at Cornell University through the joint collaboration of Brookhaven National Lab (BNL) and the Cornell Laboratory for Accelerator based Sciences and Education (CLASSE). The spring of 2018 saw the first major commissioning period for CBETA. Known as the Fractional Arc Test (FAT), this experiment bought together for the first time elements of all of the critical subsystems required for the CBETA project: the injector [3,4], the Main Linac Cryomodule (MLC), the low energy (S1) splitter line which includes several new electromagnets, a path length adjustment mechanism, and a new BPM system, as well as a first prototype production permanent magnet girder featuring 4 cells of the FFA return loop with its own corresponding vacuum system and BPM design (Fig. 1).

MEASUREMENTS AND ANALYSIS

As the beam was first being sent through the l Initial attempts at steering the beam through the center of the main linac cavities indicated an offset of the MLC with respect the BPMs on either side of the linac. In particular, manual alignment of the beam in the first cavity suggested a vertical offset of roughly 5 mm. Consequently, more detailed measurements were performed to better quantify these observations. These measurements proceeded as follows: each cavity was turned on individually (all other cavities turned off). In each transverse direction a pair of corrector magnets was used to scan the beam position on the BPM just upstream of the MLC while keeping the beam's angle constant. For each incoming beam position in this scan, the phase of the cavity was then scanned from 0° to 360° in steps of 30°, and the transverse positions on the downstream BPM (ID1BPC10) measured. If the beam enters the cavity off axis, then the cavity focusing delivers a phase dependent kick, resulting in a peridic beam displacement on the downstream BPM. The variance of the downstream positions on the BPM each direction gives was used to estimate the cavity offset, allowing for a rough centering of each position scan. Horizontal scans were performed first, in order to minimize any horizontal beam offset going into the cavity, after which vertical scan data was taken for each cavity. The voltage of the cavities was increased from 500 kV on the first cavity (RD1CAV06) and increased by 100 kV for each subsequent cavity.

Figure 2 shows the vertical position on the downstream BPM as a function of the vertical upstream BPM position for the various values of the first cavity (RD1CAV06) phase and a cavity voltage of 500 kV. The data clearly imply a linear relationship between BPM readings.

In this case, the linear transport of the beam centroid trajectory $\mathbf{u} = (y, y', 1)^{\mathrm{T}}$ through each cavity can be written as

$$\mathbf{u}_f = D(L_2)R_{\mathrm{out}}T(\phi)D(L_1)R_{\mathrm{in}}\mathbf{u}_i \equiv M\mathbf{u}_i, \qquad (1)$$

where $D(L)$ is the standard form for a drift transfer matrix and $L1$ and $L2$ are the drift lengths between the upstream BPM and cavity and cavity and downstream BPM respectively, $T(\phi)$ is the cavity transform matrix, and R_{out} and R_{in} transform the centroid position and angle into and out of the
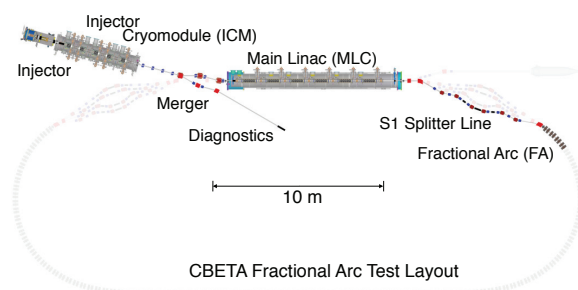
Figure 1: Schematic of the CBETA machine highlighting the components installed for Fractional Arc Test.
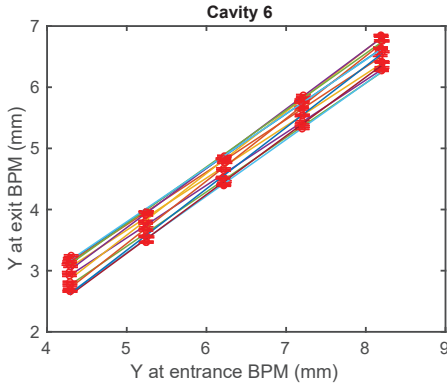
Figure 2: Example BPM data taken for the first MLC cavity with best fit lines. Each line corresponds to a different cavity phase.

offset and tilted cavity coordinate system. In terms of the cavity offset y_c and tilt y_c', these matrices take the form:

$$R_{\text{in}} = \begin{pmatrix} 1 & 0 & -y_c + \frac{L_c}{2} y_c' \\ 0 & 1 & -y_c' \\ 0 & 0 & 1 \end{pmatrix}, \qquad (2)$$

$$R_{\text{out}} = \begin{pmatrix} 1 & 0 & y_c + \frac{L_c}{2} y_c' \\ 0 & 1 & y_c' \\ 0 & 0 & 1 \end{pmatrix}, \qquad (3)$$

assuming the cavity is tilted about its center point. Note the use of the third row in the above matrices and phase space vector, which allows for instantaneous shifts in coordinates at the cavity entrance/exit. The tilt y_c' is included the analysis appears as a titled cavity provides a transverse kick from the E_z component of the cavity field, and thus contributes to phase dependent motion on the downstream BPM.

It turns out that the expression in Eq. (1) simplifies by writing the problem in terms of the "effective thin lens" cavity matrix $\tilde{T} = D(-L_c/2) \cdot T \cdot D(-L_c/2)$, which parametrizes the problem in terms of one single drift length $\tilde{L} = L_2 + L_c/2$. Ignoring the initial angle of the beam (estimated here to be $\lesssim 0.1$ mrad), the downstream position of the beam becomes:

$$y_f = y_c + M_{11}(y_i - y_c) + \left[\tilde{L} \left(1 - \tilde{T}_{22} \right) - \tilde{T}_{12} \right] y_c', \qquad (4)$$

where $M_{11} = \tilde{T}_{11} + \tilde{L}\tilde{T}_{21}$. Note that the above expression takes the form of a line: $y_f = m \cdot y_i + b$ where the phase dependent slope and intercept are identified as $m(\phi) = M_{11}(\phi) = \tilde{T}_{11} + \tilde{T}_{21}\tilde{L}$ and $b(\phi) = (1 - M_{11})y_c + \left[\tilde{L} \left(1 - \tilde{T}_{22} \right) - \tilde{T}_{12} \right] y_c'$. In order to extract the offset terms from, these terms are Fourier expanded:

$$m(\phi) = \sum_{n=0}^{\infty} m_n^{(c)} \cos(n\phi) + m_n^{(s)} \sin(n\phi) \qquad (5)$$

$$b(\phi) = \sum_{n=0}^{\infty} b_n^{(c)} \cos(n\phi) + b_n^{(s)} \sin(n\phi) \qquad (6)$$

$$\tilde{T}_{ij}(\phi) = \sum_{n=0}^{\infty} \tilde{T}_{ij,n}^{(c)} \cos(n\phi) + \tilde{T}_{ij,n}^{(s)} \sin(n\phi), \qquad (7)$$

where $\phi = 0$ corresponds to the on-crest acceleration of the cavity. Substituting these expressions into Eq. 4 and collecting like Fourier coefficients gives the following expression for the cavity offsets:

$$\begin{pmatrix} y_c \\ y_c' \end{pmatrix} = - \begin{pmatrix} m_n^{(c)} & \tilde{L}\tilde{T}_{22,n}^{(c)} + \tilde{T}_{12,n}^{(c)} \\ m_n^{(s)} & \tilde{L}\tilde{T}_{22,n}^{(s)} + \tilde{T}_{12,n}^{(s)} \end{pmatrix}^{-1} \begin{pmatrix} b_n^{(c)} \\ b_n^{(s)} \end{pmatrix}. \qquad (8)$$

Equation 8 finds the cavity offset and tilt using a combination of the data ($m(\phi)$ and $b(\phi)$) and matrix elements of the cavity ($\tilde{T}_{ij}(\phi)$), which we compute by integrating through a field map for the cavity. There may be a phase offset between our data and the model of the cavity through which we integrated, so our next step will be to find that phase offset. We do this by taking advantage of the fact that $m(\phi) = M_{11}(\phi)$. We first integrate through the cavity field map to determine $M_{11}(\phi)$, and fit the results to a Fourier expansion through the third harmonic. We then make a least squares fit of $m(\phi)$ to $AM_{11}(\phi + \phi_0) + B$ and find the parameters ϕ_0, A, B. Fig. 3 shows the result of this procedure for the slope data from the cavity 6. For that cavity, the scaling factor A was roughly 0.967 (the other cavities had A ranging from 0.942 to 1.03). The purpose of this step is only to compute ϕ_0; A and B are not used in subsequent calculations.
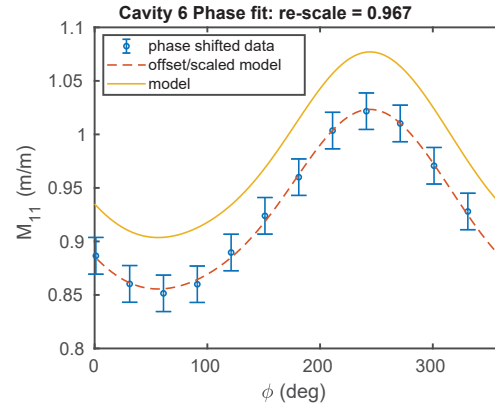
Figure 3: Example of finding the on-crest phase by scaling, offsetting, and phase shifting the model Fourier components to match the measured data. The results here show the measured data with the on-crest phase offset included, that is $\phi=0$ corresponds to on-crest in the data and model shown here.

The uncertainties shown in Fig. 3, as well as those in all subsequent calculations arise from two sources: uncertainty in the underlying BPM readings, and systematic errors due to the model being an imperfect representation of our data. The systematic errors can be seen in the linear fits that determine m and b at each ϕ. We estimate the systematic error by computing the χ^2 per degree of freedom for the line fits, assigning the systematic error to be the square root of χ^2 times the random errors, and adding that to the random error in quadrature to obtain our uncertainty estimate. The systematic errors are always larger than the random errors, and for cavity 1 by a large factor.

MC3: Novel Particle Sources and Acceleration Techniques

A12 Fixed-Field Alternating Gradient Accelerators

Now that we have the phase offset ϕ_0, we perform a discrete Fourier transform on $m(\phi)$ and $b(\phi)$, phase shifted by ϕ_0, to obtain $m_1^{(c,s)}$ and $b_1^{(c,s)}$ (Fig. 4 shows the m and b data along with the Fourier series approximation to the third harmonic). We also fit $\tilde{T}_{12}(\phi)$ and $\tilde{T}_{22}(\phi)$ to a Fourier expansion to the third harmonic. We then apply Eq. (8), with $n = 1$ (which is the dominant Fourier mode) to obtain y_c and y_c'.
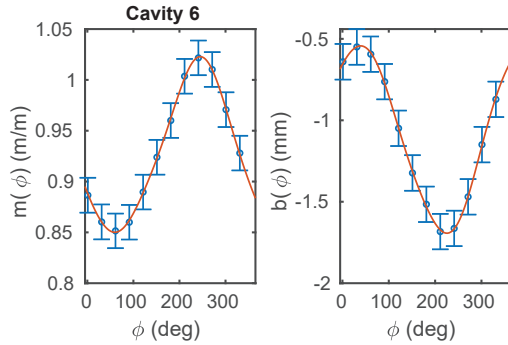
Figure 4: Example of the final fit to the slope and offset terms in Eq. (4). ϕ=0 corresponds to on-crest acceleration.

The resulting offsets and tilts are shown in Fig. 5. All of the cavity offsets are in the positive vertical direction and have a weighted average of roughly 4.0 mm, very near the rough estimate provided by operators manually trying to center the beam through the linac cavities. In particular, the large error bar on both the offset and tilt on cavity 1 indicate a greater systematic error in these particular results compared to the other cavities. This systematic error follows from the quality of the initial linear fits. We point out that this cavity was the closest to the BPM downstream of the main linac cryomodule. This results in the smallest change of the downstream BPM.

CONCLUSION

The methods discussed in this work indicate that the initial placement of the CBETA main linac cavities are on average 4 mm high with respect to the BPMs on either side of the linac. As a consequence of these results the beamline, BPMs, and main linac have all been resurveyed. These resulting survey data indicated an initial vertical survey error of up to 3 mm. The linac cryomodule was subsequently lowered by 3 mm. As of this work, additional beam based measurements of the main linac cavity positions are currently underway. Initial results, using the same analysis described here, indicate that the cavities are now near the design axis of the machine.
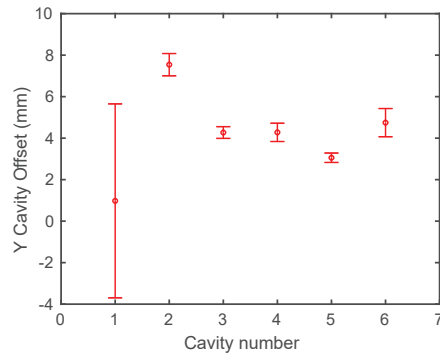
(a) Vertical cavity offsets.
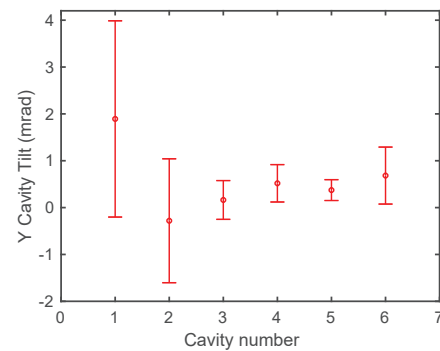
(b) Vertical cavity tilts.

Figure 5: Vertical cavity offsets (a) and tilts (b). The error estimates here include both systematic in fitting lines to the BPM data, as well as the random error in the BPM position readings.

REFERENCES

[1] G. Hoffstaetter, *et al.*, CBETA Design Report, Cornell-BNL ERL Test Accelerator, arXiv:1706.04245[physics.acc-ph]

[2] K. Halbach, *Nuclear Instruments and Methods* 169, 1 (1980).

[3] B. Dunham, *et al.*, *Applied Physics Letters* 102, 034105 (2013).

[4] C. Gulliford, *et al.*, *Phys. Rev. ST Accel. Beams* 16, 073401 (2013).